SmartSpring: A Low-Cost Wearable Haptic VR Display with Controllable Passive Feedback

Hongkun Zhang, Kehong Zhou, Ke Shi, Yunhai Wang, Aiguo Song, and Lifeng Zhu

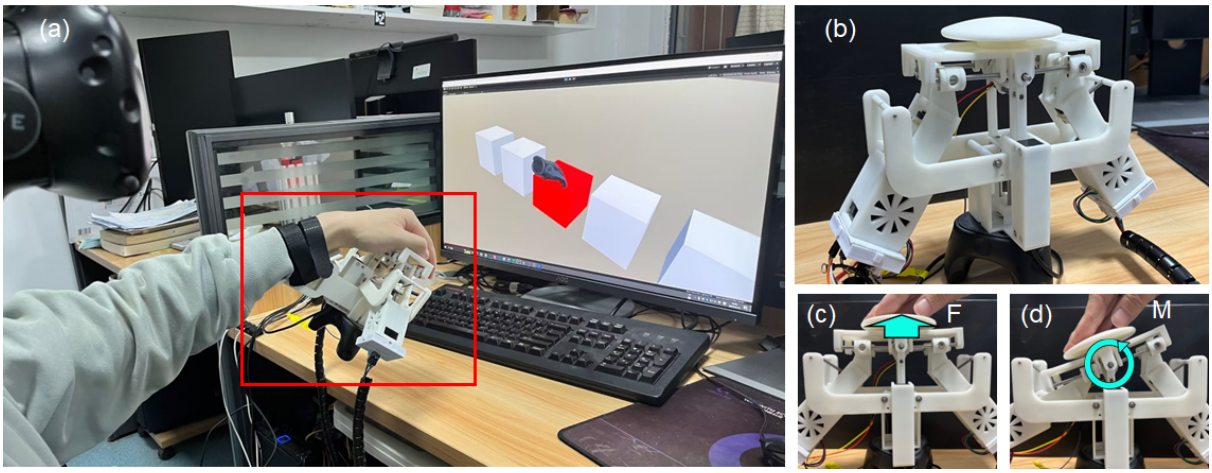

Fig. 1: We propose SmartSpring, a new passive device for haptic display. (a) The user wears the proposed SmartSpring to perceive haptic feedback. With continuous force signals from the VR scene as the input, SmartSpring intelligently updates its structure to provide desired forces, simulating the experience when pressing soft objects. (b)The prototype of SmartSpring. The spring-linkage structure, controlled by motors, adjusts the system stiffness, rendering different (c) forces or (d) torques when the user's hand is in contact with the touching pad.

Abstract—With the development of virtual reality, the practical requirements of the wearable haptic interface have been greatly emphasized. While passive haptic devices are commonly used in virtual reality, they lack generality and are difficult to precisely generate continuous force feedback to users. In this work, we present SmartSpring, a new solution for passive haptics, which is inexpensive, lightweight and capable of providing controllable force feedback in virtual reality. We propose a hybrid spring-linkage structure as the proxy and flexibly control the mechanism for adjustable system stiffness. By analyzing the structure and force model, we enable a smart transform of the structure for producing continuous force signals. We quantitatively examine the real-world performance of SmartSpring to verify our model. By asymmetrically moving or actively pressing the end-effector, we show that our design can further support rendering torque and stiffness. Finally, we demonstrate the SmartSpring in a series of scenarios with user studies and a just noticeable difference analysis. Experimental results show the potential of the developed haptic display in virtual reality.

Index Terms—Passive haptic, wearable display, virtual reality

1 Introduction

The advent of virtual reality (VR) technology has revolutionized the way users interact with virtual environments, by leveraging head-mounted displays (HMDs) to provide visual and audio feedback for an immersive experience. Haptic cues are further anticipated to enhance immersion by introducing force and tactile feedback to VR [1]. The development of light-weight and portable haptic displays [2] has enabled haptic cues to be integrated into a growing number of VR applications [3].

Among the various multi-modal haptic channels, force signals are considered one of the most important pieces of information to be conveyed in haptic feedback [4, 5]. Numerous haptic devices utilize active or passive force feedback mechanisms, which rely on various actuators and kinematic structures [6, 7]. Contrary to pseudo-tactile devices [8], which offer visual feedback, both active and passive devices have the capability to deliver more realistic and immersive tactile feedback. Although active forms of devices such as Phantom or Haption are known to be capable of providing controllable force feedback to users, stability and safety are the common issues of the active solutions [9]. During VR interactions, users may input different motion signals, and dedicated controllers should be adopted to regulate the active actuators, such as motors, accordingly to generate force feedback with high fidelity. On the other hand, active devices are usually grounded, expensive, and large for providing scalable forces, which is not friendly for VR applications, especially when the users have to move dynamically within the scene.

Passive haptics are frequently utilized in VR interactions due to their advantages in terms of mobility and safety [10, 11]. Typically, hand-controllers are enhanced to convey the sense of resistance [12] or contact [13, 14] with passive haptics by designing controllable shape-changing structures. Many passive haptic devices employ magnetorheological fluid [15, 16] or electromagnetic brakes [17], and the outputs are

- *Hongkun Zhang, Kehong Zhou, Aiguo Song, Lifeng Zhu are with the State Key Laboratory of Digital Medical Engineering, Jiangsu Key Lab of Remote Measurement and Control, School of Instrument Science and Engineering, Southeast University, 210096 P.R.China.*
- *Ke Shi is with National University of Singapore, Singapore.*
- *Yunhai Wang is with the Shandong University, P.R.China.*
- *Hongkun Zhang and Kehong Zhou are co-first authors of the article (e-mail: H.K.Zhang5813@gmail.com; zhoukh97@163.com).*
- *Corresponding author: Lifeng Zhu (e-mail: lfzhulf@gmail.com)*

Manuscript received 25 March 2023; revised 17 June 2023; accepted 7 July 2023. Date of publication 2 October 2023; date of current version 31 October 2023. This article has supplementary downloadable material available at https://doi.org/10.1109/TVCG.2023.3320249, provided by the authors.
Digital Object Identifier no. 10.1109/TVCG.2023.3320249

mostly displayed to resist the input motion from users with damping forces, which is safe during the interaction. However, the damping force generated by passive actuators is usually very large, making it challenging to precisely specify the output force continuously. As the passive forces will vanish if the user stops exerting a large force, many passive devices are restricted to provide viscous force or halting the user's input motion, which is suitable for only a few VR scenarios.

There are also attempts to integrate active and passive haptics technologies [18]. Researchers expect to improve the stability of active haptic displays [19] by incorporating a passive damper into the design of active haptic devices, which is still an expensive solution for haptics. They also wish to improve the generality of passive haptic feedback by enabling the redistribution of mass in passive haptic proxies using active motors, which is also known as dynamic passive haptic feedback [20–22]. Yet, due to the limited shape space of passive haptic controllers, the application scenarios of currents variants of passive haptic devices in VR are still restricted.

In this work, we aim to improve the design of passive haptic devices by enabling continuous force feedback instead of damping forces, while maintaining the size of the devices suitable for wearable forms. With the implementation of continuous force feedback, the generality of passive haptics is expected to be significantly expanded, allowing for more VR applications to be supported. We follow the idea of dynamic passive haptic feedback and introduce a controllable spring-linkage hybrid structure for providing continuous forces to VR users. We model the compliance of the hybrid structure and propose a method to control the system for producing target time-varying forces. We name the prototype of our solution the *SmartSpring* in this work, as the prototype device will dynamically update its spring structures to produce desired haptic information and the system itself acts like a smart spring with controllable stiffness characteristic during the interaction. The devices with our design are capable of generating versatile force signals using a new passive structure, even if the user does not exert a large force on the handle. We quantitatively evaluate the force, stiffness and torque provided by SmartSpring and design applications to demonstrate its potential in VR. This paper presents the following main contributions:

- we introduce a new design of a passive haptic display with hybrid spring-linkage structures, which is capable of conveying continuous force, stiffness and torque signals;
- we analyze the theoretical model of the new structure and design a control system to provide specified haptic information;
- we experiment a physical prototype of our design with VR applications, providing the performance of our solution with sensory data as well as the perceptional data in user studies.

2 Related Work

Haptic feedback plays a key role in sensory modalities in VR and AR [23]. In order to better facilitate user interactions in VR, haptic displays with various forms have been proposed. Various solutions are developed for providing users with the sense of force, vibration, shape, roughness, softness or even temperature in different VR applications [24]. In this work, we aim to simulate the sense of touch or contact with objects mostly through the force feedback. We list representative solutions along this line and will refer to the above surveys for more related works.

Active haptics in VR. General haptic devices that provide controllable force feedback are commonly designed using active haptics. By integrating active actuators with kinematic structures, the torque generated by active motors is converted into forces or torques that are output to user's hands [25]. Although the desktop solutions utilizing active actuators are capable of producing general force feedback, their suitability for VR applications may not always be optimal due to factors such as the fidelity and stability of the produced force, as well as the size of the haptic devices, which should be taken into consideration during the design process.

Recent attempts to introduce active haptics to VR applications include encountered-type interface. By controlling the motion of the haptic proxy using wrist-mounted active joints [18], body-mounted robot manipulators [26], or even drones [27], users may interact with real-world proxies in demand to map their contact with virtual objects in VR. As for the real-world proxy, researchers also explored the use of pin arrays to produce haptic cues by controlling their motion [28]. At the scale of fingertip, Benko et al. [29] proposed the NormalTouch, a controller capable of rendering multiple-degrees-of-freedom (DOF) force and shape feedback on the finger. This device can also display the texture of virtual objects. Other solutions based on skin-stretch include those that using wires [30, 31], deformable membranes driven by electroactive elastomer [13, 14] or compressed air [10, 11]. However, it is difficult to precisely quantify the force feedback provided by those encountered-type contact or skin-stretch solutions.

Passive and dynamic passive haptics. By designing passive structures to simulate desired shape or material properties, haptic devices may display variable elasticity at a low cost. Customized manufacturing of virtual object is a common way to simulate the true haptic feedback. For example, Teng et al. proposed to fold and seal the non-elastic PE sheets, and then inflate it to display objects such as spheres, cylinders or boxes [32]. Whitmire et al. introduced a reconfigurable wheel that can switch passive objects with different textures, allowing the rendering virtual objects with similar material properties [33]. Yang et al. designed a reconfigurable display, which can adjust the DOF of a pad by selectively tightening or loosening the cables [34]. However, the displayed shape space is limited and they may not be inconvenient for providing specified force signals.

Shape-changing proxies are also commonly seen in VR interactions. The concept is to dynamically adjust the shape of the passive haptic proxy grasped in hands, so that the user perceives similar shape or interaction properties of the virtual objects, which is also known as dynamic passive haptics. Researchers have proposed dynamically adjusting the center of gravity [20, 21], the shape distribution [35], the stiffness distribution [36] or shifting the weights of handheld controllers [22, 37]. However, the output force provided by these solutions is hard to quantify. While these methods can roughly simulate haptic feedback when holding different virtual objects, they cannot accurately reproduce desired forces to the user.

Typical passive haptic devices introduce controllable damping modules to provide the contact sensation. Limiting the motion of users' fingers is an effective method for rendering specific shapes. Methods for damping the users' finger motion include the programmable multi-string system [38], the fiber jamming glove [39], the brake-based system [12, 40]. Strasnick et al. presented a system that utilizes the ball-and-socket joint lock linked to two handheld controllers to produce passive haptics for bimanual interactions in VR [41]. While these passive solutions are safe and capable of producing varying levels of resistance force, they are mostly suitable for providing frictions and may not perform well if the users stop moving their hands during the interaction.

Springs have been integrated into mechatronics and robotics as a reliable passive element for generating forces and controlling the exerted force [42–44]. For haptic applications, Mike et al. [45] proposed a passive system that utilizes springs to generate passive forces and brakes to control the damping of the system. However, due to the one-DOF design of the system, the haptic feedback is limited to applications where the user grasps virtual objects. Mohammad et al. [46] proposed the BpVSJ, a passive haptic interface with variable stiffness. However, the system had a complex structure of springs and only allowed for switching between a discrete set of variable stiffness. Additionally, it was grounded and had a large size, making it unsuitable for use as handheld controllers in VR applications.

In our design, force feedback is primarily provided by springs. The compliance of these springs enables the device to mitigate hand jitter, thus enhancing the system's stability. In this regard, the system may be thought as a special type of active haptic device. More precisely, SmartSpring adheres to the principle of dynamic passive haptic [20] and is designed as a hybrid active-passive device, wherein the spring-linkage structure serving as a dynamic passive module for force generation. Furthermore, since motors are adopted to adjust the configuration of the spring-linkage structure rather than directly providing forces, Smart-

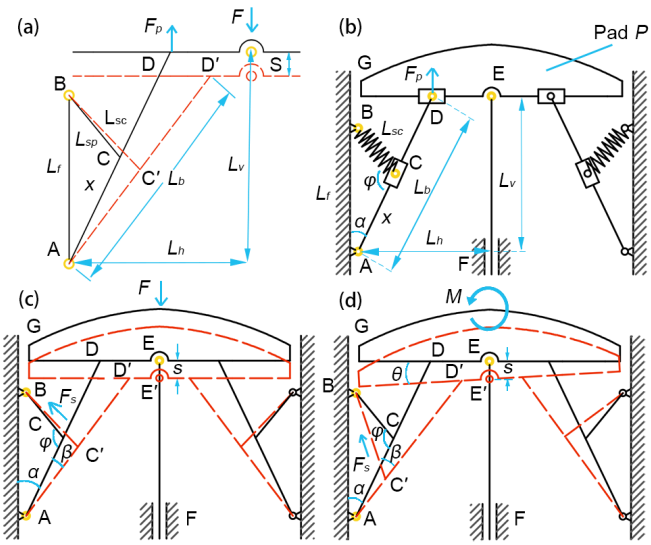

Fig. 2: (a) The kinematic diagram of the left force-generating unit based on a spring-linkage structure. (b) The schematic diagram of the structure at the initial state. Pressing SmartSpring with (c) symmetric or (d) asymmetric movement of the two force-generating units.

Spring can be regarded as a nonlinear spring with tunable stiffness. And the dynamic passive device performs fairly with a low-level intervention of open-lopp control. As a result, we maintain our categorization of SmartSpring as a passive device in this study.

Table 1 summarizes the comparison between passive displays in terms of rendering specific force. One distinguishing feature of SmartSpring is its capability to provide haptic experiences that go beyond mere damping forces. Additionally, SmartSpring offers a wide range of force outputs, thus enabling the display of rich elastic forces and expanding its potential applications.

3 Method

In this work, we present SmartSpring, a device designed to provide haptic feedback of virtual objects on the palm to enhance realism of VR experiences. We begin by discussing the design considerations before detailing the working principle and structure of the device. Next, we formulate an analytic model of the designed mechanism and use it to design three haptic modes for the proposed SmartSpring.

3.1 Design Considerations

To create a wearable device capable of providing versatile and realistic haptic feedback for VR applications, we take into account the following design considerations:

Passive haptics. Our primary aim is to create a passive haptic device, as it offers several advantages such as continuity, stability, safety, low power requirements, low complexity, and low latency. Moreover, passive devices typically offer a higher force per device weight and cost compared to active devices [45]. Additionally, we expect to create a lightweight design for the haptic display to ensure its suitability for virtual reality applications.

Controllable haptic rendering for VR interaction. In virtual environments, virtual objects may have non-constant stiffness, which can result in users receiving continuously varying force feedback when interacting with these objects. To enhance realism, it is essential to provide general force feedback with real-time control. With this in mind, our goal was to precisely display target force signals in a range when users freely move the controllers, without limiting the haptic feedback to only damping forces.

3.2 Working Principle

We introduce a hybrid spring-linkage structure as the passive haptic proxy to produce controllable force feedback, as illustrated in Figure 2(b). By controlling the layout of the springs within the structure, we can generate desired force on a touching pad linked to the spring-linkage mechanism. Our work is inspired by serial elastic actuators (SEAs) [47, 48], which are used to generate controllable forces with a system of springs and actuators. However, instead of a serial layout of the spring and actuator, we built our system with a spring-linkage structure, which uses actuators to control the layout of the passive structure, rather than actively generates force from the actuators. Spring-linkage mechanism has also been applied to the constant-force end-effector [49]. We adapt the structure to providing rich force feedback and introduce a haptic display for VR based on the structure. In addition, we exploit the compliance of the structure and propose to provide force, stiffness, torque feedback with this augmented design.

In Figure 2(b), the initial state of the SmartSpring is shown. The pad P is in a fixed rest position with the determined length between EF,denoted as L_v. When the pad is pressed down, forces are exerted on the user. The SmartSpring consists of two symmetrical spring-linkage components, as shown in (Figure 2(a)). Each spring-linkage component comprises a connecting rod AD, on which a slider C is driven by a motor to move along the line AD. A spring is attached to point B on the side and linked to the control slider C, enabling the length and direction of the spring BC to be adjusted with the slider's motion. This creates passive force on the linkage AD.

To constrain the force output on the pad P, a slider D is introduced on the rail at the bottom of the pad. The force transmitted by the linkage AD is perpendicular to the bottom of the pad P. The above linkage, spring, and sliders form one of passive force-generating units, and the force-generating unit at the other side is installed symmetrically. The slider F is used to limit the prismatic pair of the pad P in the horizontal direction, allowing the point E to move only in the vertical direction. The device consists of 9 revolute pairs, 5 prismatic pairs and 2 springs. Then the DOF of the device is $F_D = 3n - 2P_l - P_h$, where n is the number of moving links, P_l and P_h are the number of low pairs and high pairs that constrain the motion of the links, respectively. Therefore, considering the pad P as the end-effector, the SmartSpring has two DOFs, which are the vertical translation of the pad P and its rotation around the point E. When the user casually touches the pad, it will be pressed down or rotated, with the sliders driving the springs to be compressed or stretched, generating elastic forces on the rod AD at the left and right side. If we constrain the two force-generating unit to work symmetrically, a resultant force F_p will be generated on the pad, as illustrated in Figure 2(c). Alternatively, if we allow the two force-generating units to update asymmetrically, the unbalanced forces on the rod AD at each side will produce torque feedback on the pad P, as shown in (Figure 2(d)).

3.3 Force Modelling and Haptic Output Analysis

Now we will analyze the system stiffness and derive the generated force/torque based on the designed structure. Our derivation is mainly based on the force and torque balance equations on the rod AD. By combining these equations with the geometric constraints in the designed structure, we can express the output as a function of the design parameters. The detailed derivation is presented in the Appendix A, and we will directly present our models and analyze them in this subsection.

As shown in Figure 2(a), according to the force balance and geometry relations, the output force F_p from one force-generating unit on vertical direction is computed by

$$F_p = k\frac{xL_f}{L_b} + \frac{xL_f}{L_b}\cdot\frac{F_0 - kL_{so}}{T} \tag{1}$$

$$T = \sqrt{x^2 + L_f^2 - 2xL_f(\cos\alpha - s/L_b)}, \tag{2}$$

where x represents the length of AC', which is controlled by the position of slider C, L_b is the length of rod AD, L_f is the length of frame AB, L_{so} is the spring length when the SmartSpring is in the initial state,

Table 1: The comparison of the passive displays for rendering specific force

Display	Output Range	Weight	Application
Frediani et al. [14]	0-1N	6g(Single finger)	Pinch soft objects by fingertips
Kovacs et al. [18]	0-5N	188g	Grasping, catch, or throw an objects
Salazar et al. [31]	0-3N	-	Press objects by single finger
Sinclair et al. [45]	0.2-20N	-	Damping force to single finger
Ours	0-20N	710g	Press soft objects by palm

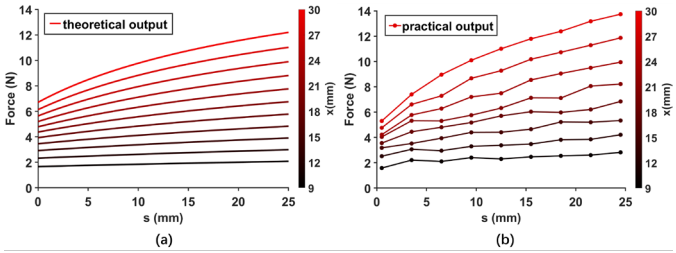

Fig. 3: (a)The force-displacement workspace of one force-generating unit of the SmartSpring. (b)We test the output from our prototype system, which well matches with the theoretical model.

with L_{so} longer than the rest length of the spring to provide an initial force F_0, α is the angle between AB and AD when the SmartSpring is in the initial state, k is the constant stiffness of the spring, and s is the displacement measured by a sensor. In Equation 1 and Equation 2, the parameters $\{L_b, L_f, \alpha, k, F_0\}$ represent the set of design parameters that are determined during the design process, while s is measured by a sensor in real-time. According to the variable s, the motor can adjust x to output the desired force F_p.

Based on the force output model, we analyze the force-displacement curves of one force-generating unit with different configurations of x, as shown in Figure 3(a), using the default design parameters listed in Table 5. From the plots, we observe that each force-displacement curve is nearly linear with a low slope, where the range of the gradient is within 0.014 N/m to 0.453 N/m. We also used a force sensor to sample the output of one force-generating unit and found the practical output well follows our theoretical model, as shown in Figure 3(b). The details about how we sample the outputs will be presented in the next section.

As shown in Figure 2(c), when the two sliders work symmetrically, the output forces from the two springs are balanced along the horizontal direction. Therefore, the resultant force F applied on the touching pad P is computed as

$$F = 2F_p. \tag{3}$$

Given a target force F, along with the known design parameters and the measured displacement s, we can determine the controlled length x by solving Equation 1,Equation 2, and Equation 3 using Newton's Method. In this case, we obtain our model describing how to quantitatively adjust x in order to generate the desired force F in response to the real-time measured displacement s.

When the two sliders operate asymmetrically, the output forces generated by the two force-generating units differ. The imbalanced output forces F_{p_1} and F_{p_2} for each side will provide a torque exerted on the end-effector. In this mode, without restricting the rotational motion of pad P, it typically have an angle θ deviating from the horizontal direction when the hand casually holds the pad, as illustrated in Figure 2(d). Due to the inclined pad, the rotation angles of the two rods and displacements of the two sliders differ. Upon analyzing the output force from each force-generating unit, we derive the output torque M, calculated as:

$$M = F_{p_2} l_2 - F_{p_1} l_1, \tag{4}$$

where l_1 and l_2 denote the left and right force arms, originating from the left and right slider D_1 and D_2 and extending to the center of pad E. Comprehensive derivations for computing l_1 and l_2 can be found in Appendix A. Similarly, based on the measured displacement s and rotation θ gathered from sensors, we can determine the displacement of the sliders C_1 and C_2 on each side using the above equations. This process allows us to obtain the motor control signals necessary to generate the target torque M.

3.4 Interaction

Based on the theoretical analysis, we propose three haptic modes of SmartSpring.

Force display mode outputs a target force F, which is transmitted to the device from virtual environments. In this mode, we ensure that the two force-generating units work symmetrically. As discussed in Sect.3.3, the device controls the motor on each side to adjust the length x, thereby generating the desired force F on the pad P. During interaction, the user casually hold the pad. The static holding gesture generates a slight displacement of the touching pad, activating the force display mode. In the virtual environment, the user's hand often exhibits unnoticed movements and subtle waving, leading to the hand's location on the pad not being perfectly fixed. These movements are referred to as involuntary hand movements. To feedback a target force and make it independent on the involuntary movements, the displacement sensor measures the position of hand, and SmartSpring dynamically updates the spring-linkage structure (the control length x) to compensate for the relative motion of the hand. Due to the low slope of the force-displacement relationship in our model, the dynamic adjustment of x remains slight, enabling the motors to follow it effectively. On the other hand, if the target force input to SmartSpring is a continuously varying signal, our system can actively update the spring-linkage layout to reproduce the desired force.

Stiffness display mode outputs varying stiffness for the entire spring-linkage structure, rendering desired stiffness of the virtual objects in VR. As the spring-linkage structure essentially forms a stiffness-tunable spring connected to the touching pad, SmartSpring naturally supports displaying varying stiffness by adjusting the spring-linkage layout. Given a target stiffness k_p as the desired system stiffness, we solve $\frac{dF}{ds} = k_p$ and determine the control length x. Users can actively press the touching pad to perceive the desired stiffness. By leveraging the passive haptics provided by springs, the force is stably varying in response to the displacement of the pad, displaying realistic elastic features when users press the pad. In addition to produce specified stiffness along the vertical direction, we may also lock the adjusted control sliders, allowing SmartSpring to function as a passive proxy. Users may press the touching pad from different sides to perceive varying levels of stiffness on each side. We expect this full passive solution will stably simulate the experience of pressing soft objects, as shown in Figure 8(c), and will validate its performance in Section.5.

Torque display mode outputs desired torque on the touching pad. In this mode, the two sliders are allowed to work asymmetrically, generating a torque on the user's hand. Similar to the force display mode, users may perceive the torque while casually holding the pad. The SmartSpring will sense the rotational displacement θ of the pad, prompting the motor at each side to adjust the layout control slider and generate the target torque.

4 Evaluation

We built a prototype of SmartSpring and conducted quantitative experiments to verify our model in this section.

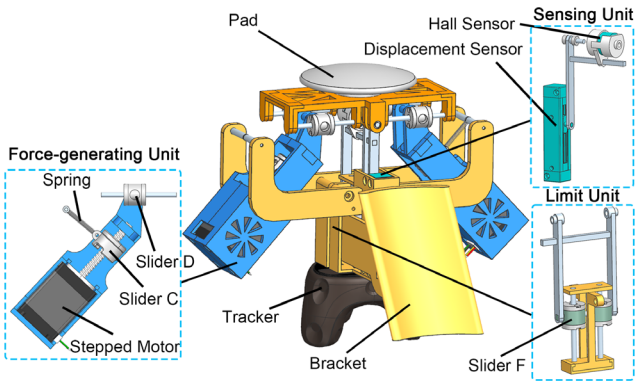

Fig. 4: The 3D model of SmartSpring.

Table 2: Key performance parameters of SmartSpring

Parameters	Value	Units
The length of the rod AC x	9 - 30	mm
The vertical displacement of the pad s	0 - 25	mm
The output force range (theoretical)	0 - 21	N
The output force range (recommended)	0 - 20	N
The output torque range (theoretical)	0 - 256	mNm
The output torque range (recommended)	0 - 250	mNm

4.1 System Implementation

As show in Figure 4, our SmartSpring prototype is composed of a touching pad, two force-generating units, a sensing unit, a limit unit, a bracket, and a tracker. The force-generating units employ the spring-linkage structure to drive the pad for haptic rendering. The sensing unit measures the vertical displacement and rotation angle of the touching pad. The limit unit is introduced to limit the movement of the pad in the horizontal direction. The bracket serves as the supporting platform, allowing users to wear SmartSpring on their forearm. The tracker is mounted to provide the pose information of the controller to VR applications. The wearable design has been tailored to ensure that users naturally hold the touching pad, generating a displacement of about 12.5 mm in the rest pose. In this case, the haptic display is triggered when it upon mounting.

In our implementation of the prototype system, we use stepper motors (28HS4401-65N2-50, UMot) to drive the stainless-steel tension springs with a stiffness of 1.3 N/mm to adjust the feedback force. Linear bearings (LMK6UU, BKD) and ball bearings (MR95, YXVSY) are used for translational and rotational pairs, respectively. A linear displacement sensor (KSF-25, MIRAN) is mounted in the middle of the SmartSpring to sense the vertical displacement of the contacting pad. Additionally, a hall sensor (P3015S-V1-CW360, OEM) is embedded in pad P to measure its rotation angle. Moreover, the stepper motors are controlled by motor drivers (UM242, UMot) and powered by switching mode power supply (LM100-22B24, MORNSUN).

We calibrate our system before using it in VR scenarios. The springs in the initial state are pre-stressed to counterbalance the weight of the touching pad. Upon measurement, the practical ranges of haptic output reach 25N for symmetric output and 275mNm for asymmetric output. The rotation speed of the stepper motor is set as 15.6 rounds per second, with one round corresponding to a 2mm displacement of the slider. It takes approximately 0.67s for the slider to traverse from its lowest position to its upper bound. However, VR interactions seldom require sliders to suddenly translate for a long distance. The system effectively renders force signals from VR scenes. Additionally, to present the stability of the proposed hybrid spring-linkage structure, we only employ an open-loop control with an update frequency of 20Hz. The controller receives displacement and rotation angle, then outputs haptics.

The overall system diagram is illustrated in Figure 5. The virtual

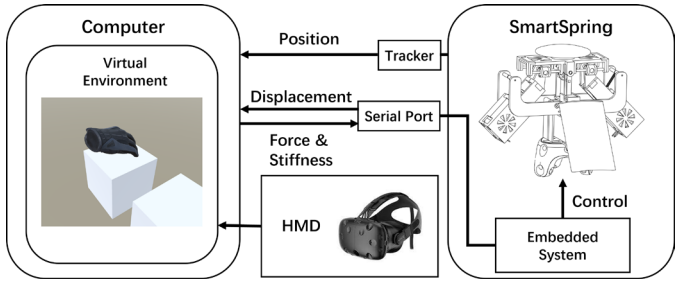

Fig. 5: The overall system of VR interaction with SmartSpring.

environment operates on a desktop computer, while an embedded system controls the motors and communicates with the computer via a serial port. Visual feedback from the virtual environment is sent to users through the head-mounted display (HMD). During runtime, virtual hands move according to the tracked pose, scaled appropriately. When virtual hands press the objects in the virtual scene, the haptic rendering module calculates the desired force, stiffness, or torque and transmits the haptic data to SmartSpring. SmartSpring then update its passive structure to display desired haptic information to the user. In our prototype, the Arduino Mega 2560 is selected as the embedded system. The virtual environment, designed using the Unity Engine, runs on a desktop equipped with an Intel Core i7-11700KF CPU and an NVIDIA GeForce RTX 3090 graphic card. We use the HTC VIVE, along with its HMD and VIVE tracker, as the VR device, providing visual cues and tracked poses during interaction.

4.2 Constant-Output Experiments

4.2.1 Experimental Procedure

In this experiment, we validated the performance of the output force range and its precision. The SmartSpring was oriented upwards and configured to output constant forces and torques. For each constant output, the pad of the SmartSpring was pressed with a displacement s from 0mm to 25mm, then released. The process was repeated five times. During the torque experiment, since the range of rotation angle varied with respect to the displacement of pad, we rotated the pad at random angles within the feasible range while pressing down. The actual forces and torques were measured by a pair of force sensors (DSZ-100, DECENT) set under the pad during these operations. According to the practical range of output, we tested the force within a range of 1-25 N with a 1 N interval, and the torque within a range of 25-275 mNm with a 25 mNm interval.

4.2.2 Results

The results of the constant output rendered by SmartSpring are shown in Figure 6, with black dotted lines are references of target outputs. In Figure 6(a)(c), we plotted the average of all measured force and torque signals under different displacements of the touching pad, where the color of the polylines indicated the actual force or torque to approach the desired constant outputs. From the results, we find that the practical output from SmartSpring closely follows the input target within the range of 2-8 N for constant force display and 50-200 mNm for constant torque display. Because the force and torque rendering model is triggered when the touching pad was pressed down, tiny displacement s of the pad may not effectively provide the haptic feedback. Especially when the target force or torque is large, the rendered haptic signal will be better perceived when the pad is pressed with a noticeable displacement. As we designed our prototype to generate the displacement s about 12.5 mm when wearing it, the recommended range for the force and torque display reached 0-20 N and 0-250 mNm.

In Figure 6(b)(d), we also show the distribution of the haptic feedback when our device is used to follow constant outputs. We used box plots to display the distribution of the rendered force or torque in the measurements. Each curve represented data from a single pressing down pass. We plotted the measurements when the output force was

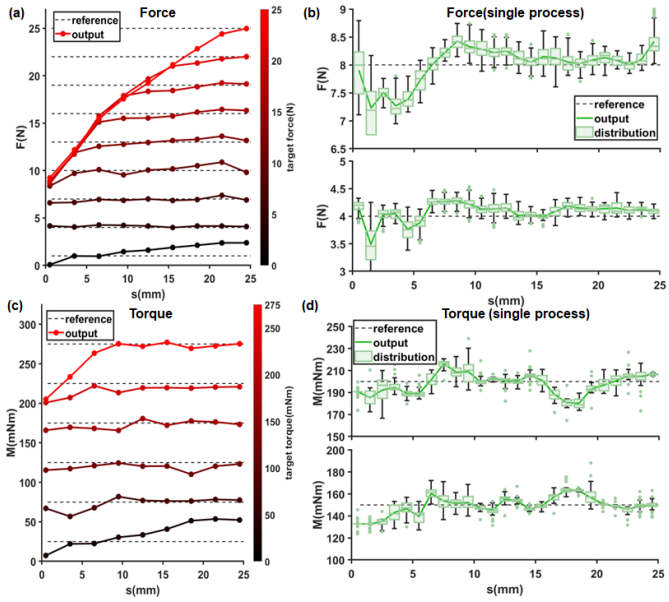

Fig. 6: The results of the constant-output experiments. We show the actual force (a) and torque (c) to reproduce target constant values under different displacement of the touching pad. We also plots several examples to show the distribution of the output forces (b) or torques (d) in constant-output experiments.

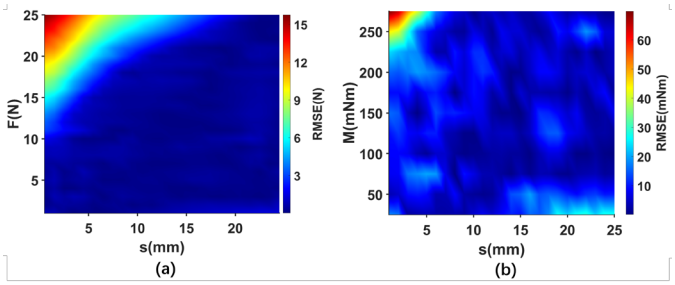

Fig. 7: The RMSE of the output forces and torques in the constant-output experiments.

Fig. 8: (a) We measure the force-displacement curve when touching a sponge cube. We simulate the experience for pressing the sponge vertically or with a slope (b) using SmartSpring (c).

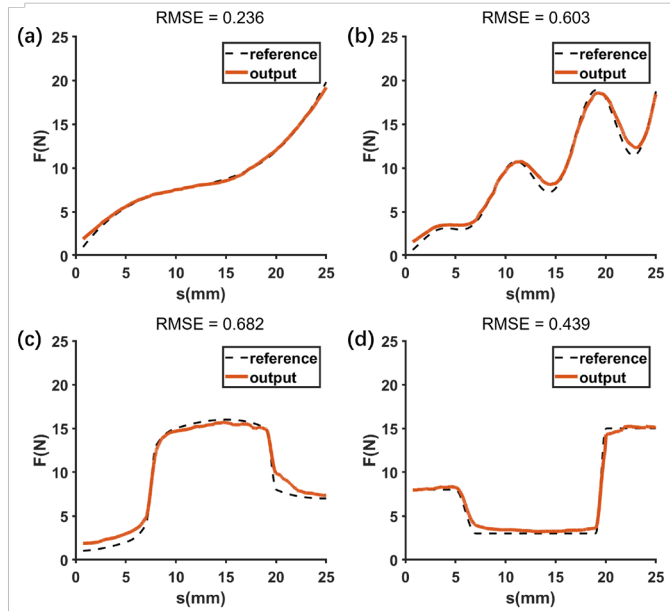

Fig. 9: The results of the variable-output experiments. Our haptic device produces continuous force feedback that well follows the desired forces.

targeted to be 4N and 8N in Figure 6(b). Similar results were observed for other constant output within our recommended working range. Two sets of representative plots for torque feedback are shown in Figure 6(d). The overall standard deviation of the rendered force or torque is about 0.297N or 9.522mNm in our experiments, which also indicates how well SmartSpring follows the desired constant force.

We further computed the root mean square error (RMSE) for all the measured outputs $d_{RMSE}(F_m(F,s),F)$, where $F_m(F,s)$ is the measured output when rendering the constant target F under the displacement s. The errors were mapped to colors and plotted in Figure 7. In the overall expected working range, the RMSE of force display mode was 3.41 N, and that of torque display mode was 12.32 mNm. In the recommended working range from our experiment, the RMSEs were 0.49 N and 8.55 mNm, respectively. It is important to note that the force sensors used to measure the data introduced random errors at a level of 0.34 N. Taking this into account, we observed that SmartSpring was capable of producing stable force or torque feedback in the experiment.

4.3 Variable-Output Experiments

4.3.1 Experimental Procedure

For validating the performance of SmartSpring in varying force output, we set several irregular force output curve to the proposed display in this experiment, as shown by the dotted curves in Figure 9. We commanded the desired force $F(s)$ with respect to the displacement s to SmartSpring and pressed down the touching pad to measure the actual force output using the same settings in subsection 4.2. In this experiment, we also prepared a force-displacement curve from a real sponge, as shown in Figure 8 (a). We sampled the displacement and the elastic force when pressing the sponge in a quasi-static way. The displacements was measured by a linear guide rail slide module, and the force was measured by the force sensors (DSZ-100, DECENT). The obtained force-displacement curve was shown as the dotted curve in Figure 9(a).

4.3.2 Results

The measured output force with respect to the displacement is plotted as the red solid curves in Figure 9. The RMSE for each experiment is also shown at the top of each subfigure. We found the generated force of SmartSpring closely followed the specified variable output, with the RMSE being only about 0.5N in our experiments. We also examined the variable torque feedback and observe similar performance, with the RMSE being about 10.4mNm. The results validated the capability of SmartSpring for continuous haptic feedback.

5 User Study

We conducted two user studies to verify the perceptual performance of SmartSpring in VR applications, and a just noticeable difference (JND) analysis to further illustrate the haptic performance of stimuli perception. In the first experiment, participants interacted with virtual objects

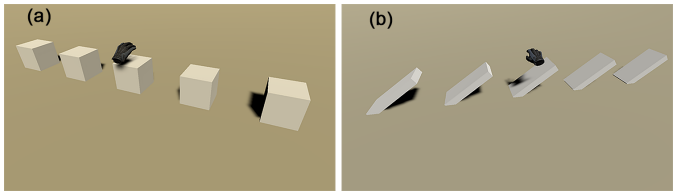

Fig. 10: The (a) elastic cubes and (b) slopes with different stiffness in VR are used to test the perceptual experience of the haptic feedback produced by SmartSpring.

Fig. 11: Confusion matrices summarizing the results from the user study in distinguishing levels of force, stiffness and toroque. The elastic objects are arranged as A, B, C, D and E by stiffness from small to large. Each row shows the total number of selected order in the 10 sets of the study.

of different hardness levels. We investigated whether the participants could discriminate these virtual objects through force, stiffness, and torque feedback from SmartSpring. In the second experiment, we used SmartSpring to simulate pressing a sponge cube with a nonlinear force-displacement curve. Users pressed both a real and a virtual sponge using our device, and the objective was to determine whether the haptic perception using our system was similar to pressing a real sponge. Furthermore, we estimated the lower bound of stimuli difference by the JND analysis in three levels of force feedback.

5.1 Participants and Apparatus

We recruited 16 healthy participants (13 males, 3 females) to take part in the virtual objects discrimination and the sponge simulation experiment. Their ages ranged from 20 to 25 (mean:22.6, standard deviation: 1.3), and they were all right-handed with normal or corrected-to-normal vision. 6 of them had experience in playing with VR applications. In the two experiments, participants wore the SmartSpring and HMD to interact with the virtual objects in the VR scenes. In the second experiment, the participant were also asked to press the real sponge shown in Figure 8 to compare the haptic perception with the one provided by SmartSpring.

5.2 Design and Procedure

Procedure. In the first experiment, we aligned ten virtual objects within two distinct virtual scenes, as shown in Figure 10. Five cubes were used to verify the force and stiffness feedback, while five slopes were used to check the torque feedback. The edge length of each cube measured 200mm, and the rotation angle of the slope platform was set at 34.5 degrees. The five cubes and slopes, characterized by varying stiffness, were placed in a random order. Upon interacting with these objects in the virtual environment, we mapped the displacement to different forces or torques, subsequently sent the desired force or torque signal to the SmartSpring. We proceeded to investigate the three modes of SmartSpring via the following ways.

Force display mode. Each user held SmartSpring and maneuvered in such a manner that the virtual hand pressed the virtual cube. The pose of hand was input to the VR scene by the tracker attached to SmartSpring. According to the position of virtual hand, each virtual cube underwent deformation and exerted virtual forces according to its stiffness. In our experiment, the stiffness of each cube was distributed equally within the range of 0.1N/mm to 0.25N/mm. The force displayed by SmartSpring when pressing the mth cube at time t was represented as $F_t = k_m d_t$, where k_m denotes the stiffness of the mth cube and d_t is the deformation of the cube at time t.

Stiffness display mode. Participants also interacted with the virtual cubes in this mode. Due to the possibility of users moving or actively pressing the touching pad during the stiffness feedback mode, visual cues were provided. The touched cube deformed in response to the tracker's pose and the displacement measured by the sensor embedded within the SmartSpring. In the experiment with the stiffness feedback, the target stiffness sent to SmartSpring was equally spaced, ranging from 0.2 N/mm to 1 N/mm.

Torque display mode. Participants rotated the virtual slopes, and the SmartSpring provided torques according to the rotation angles of these slopes. The stiffness of slopes was uniformly distributed within the range of 100 mNm/rad to 1000 mNm/rad.

It is essential to note that the deformation of the each cube, given the same displacement, remained consistent within the virtual scene. Consequently, we did not create distinct visual cues for distinguishing the stiffness of each object. Instead, we relied only on the haptic feedback provided by the SmartSpring to enable users to distinguish objects with different levels of stiffness. Similarly, the rotation of each slope was also simulated to provide the same visual feedback. Participants were allowed to freely press the cubes or slopes or take a rest whenever needed. Finally, they were asked to rank each object according to its perceived stiffness.

In the second experiment, we used SmartSpring to simulate the haptic interaction with a sponge cube. We used the same configuration described in subsection 4.3 to render the elastic force, wherein the force-displacement curve was derived from sampling the real sponge using force and displacement sensors. Additionally, we prepared the real sponge and invited the participants to press it. They were allowed to alternate between the real-world and VR interactions several times until satisfied. The participants were asked to press down steadily in each trial. For alleviating the influence of tactile differences between the pad and sponge, we covered a touching pad on the sponge cube, as shown in Figure 8. Additionally, to objectively illustrate the realism of simulation, we randomly selected four pairs of complete pressing processes and compared the force feedback of each pair in a piece-wise manner.

Measurements. In the first experiment, we recorded the ranking results for each participant and counted the number of correct rankings to form a confusion matrix, indicating whether they could effectively distinguish between different objects using the haptic feedback provided by SmartSpring. Furthermore, similar to the subjective measurements in [50], we directly had the users rate their perceptual experience to assess several aspects what we care for the performance of SmartSpring. Participants received a questionnaire with six questions after the experiment. Each question was to be answered using a 7-level Likert scale (1:strongly disagree to 7: strongly agree), as showed in Table 3. The Q1 to Q4 pertained to the first experiment and were concerned with the rendering precision, continuity, stability in passive haptic, and dynamic performance associated with SmartSpring. Meanwhile, Q5 and Q6 related to the second experiment.

5.3 Results

The results of the first experiment with 16 participants were summarized in the confusion matrices, as shown in Figure 11. We count the frequency at which each object was correctly ranked by participants and plotted these frequencies in the matrices. Thus, the minimum frequency is 0, and the maximum frequency is 16. Based on the results of experiments, we find the total success rates for force, stiffness, torque feedback were 95%, 100% and 80%, respectively. These results demonstrate that SmartSpring is capable of generating different haptic feedback, which can be discriminated by users. Furthermore, the results indicated that the torque feedback was not as effective as the

Table 3: The questionnaire in our user study

No.	Question
Q1	Is there a significant difference between different levels of haptic feedback?
Q2	Is the variation of haptic feedback continuous and smooth?
Q3	Is there unexpected change of haptic feedback?
Q4	Is there no latency of haptic feedback during experiments?
Q5	During pressing, is the haptic perception using SmartSpring similar to that of the real sponge cube?
Q6	Is the haptic feedback perceived to be similar to a real sponge when the pad is tilted?

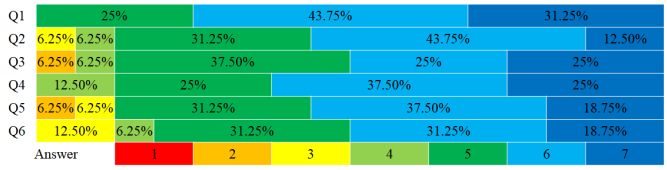

Fig. 12: The answers to the subjective questionnaire.

force and stiffness feedback in the discrimination experiment. This was due to the lower precision and smaller workspace in the torque display mode when compared with the other two output modes, as previously measured in the study. However, with a success rate of 80%, the torque feedback was still sufficient higher than the success rate of random rankings of five indices.

The questionnaires in the discrimination experiment were collected, and their results were listed in Figure 12. Generally, participants provided positive feedback in terms of the perceptual experience when using SmartSpring. As the main function of the SmartSpring, participants thought our device successfully generated variable haptic information, enabling them to perceive soft objects effectively. Moreover, the answers of Q3 indicated that the haptic device performed relatively stably. The involuntarily hand movements might introduce an unnatural haptic feedback experience if the system was unstable, while we got positive feedback of Q3. The passive structure was the primary factor contributing to this advantage. Q2 and Q4 revealed if there were any unexpected vibration or latencies in the haptic outputs. These problems were mainly limited by the performance of the stepper motors. However, according to the statistics of success rate and the overall questionnaire from the first experiment, it can be concluded that the above issues did not significantly hinder participants' ability to accurately perceive haptic outputs generated by SmartSpring.

The answers of questionnaires administered in the simulation of touching a sponge showed that SmartSpring was effective in simulating the experience of touching soft objects. The results of Q5 described that SmartSpring worked well in simulating the nonlinear stiffness presented in Figure 8. The haptic perception using SmartSpring in a VR scene was considered similar to pressing the real sponge cube. Note that our device is capable of reproducing a rich set of material properties featured as various linear or nonlinear force-displacement curves $f(s)$, while other passive solutions may only provide a finite number of linear stiffness [46]. Moreover, when a hand applied non-uniform pressure distribution to tilt the pad while pressing the sponge cube, the hand would received a torque to help restore the surface of the cube to its rest shape. The result of Q6 reflected that SmartSpring was able to simulate the phenomenon of elasticity using the two force-generating units.

Within the sponge simulation experiment, we compared the force feedback between SmartSpring and the real sponge in four pairs of completed pressing processes. We checked the differences between the displayed force by SmartSpring and the measured force when pressing the real sponge, as the objective insights to reveal the perceived realism of SmartSpring. In Table 4, we show the distribution of the differences using rooted mean square error at different ranges of displacements. Before inspecting the differences, we also normalized the measured signal

Table 4: The objective clues of simulation

	Error(N)				
s(mm)	[0, 5)	[5, 10)	[10, 15)	[15, 20)	[20, 25]
P1	1.43	1.06	0.53	0.62	1.57
P2	1.27	1.15	0.92	0.71	2.32
P3	1.95	0.70	1.11	1.68	2.28
P4	1.55	1.32	0.46	0.92	3.13

using dynamic time warping [51] to account for different length of the signals. The error data further highlight the satisfactory performance of SmartSpring in simulating the sponge press experiment. Notably, the segments [0, 5) and [20, 25] exhibit slightly larger errors compared to others, which is consistent with the observations in Figure 9(a).

After the user study, we interviewed the participants and gathered their feedback. Overall, the participants express that the haptic feedback from SmartSpring was vivid and enhanced the sense of immersion in VR interactions. Four participants mentioned that they had occasionally experienced artifacts, such as high-frequency vibrations, but they acknowledged that the impact of these artifacts was minimal and did not significantly affect their overall experience using the system.

5.4 JND Analysis

To provide further insights into the performance of SmartSpring, we conducted an experiment to estimate the JND of the device in force display mode. The experimental procedure closely followed the methodology employed in previous studies [17]. We selected three reference force levels of 5N, 10N, and 20N. Based on a pilot study, we determined that a 20% difference in force was easily discriminated by participants. Each participant completed six trials for each reference force, resulting in a total of $16 \times 6 \times 3$ trials.

The results of the JND analysis revealed average just noticeable differences of 13.31%, 10.59%, and 9.44% for the 5N, 10N, and 20N reference forces, respectively. These findings indicate that the performance of SmartSpring is generally satisfactory, as the JND values fall within an appropriate range that well aligns with existing tools [36].

6 Application

In this section, we present several additional applications more than rendering the haptic perception of a soft sponge, which leverage its capability to generate continuously varying force feedback.

Buoyant Force. Imaging the scenario shown in Figure 13, where a wooden block with varying cross-sectional area is floating in water. When people press the block steadily into water, the buoyant force exerted on the hand changes based on the cross-sectional area of the block (Figure 13 (c)(d)). Once the entire volume of the block is immersed in water with the hand pressing it statically, the buoyant force remains constant (Figure 13 (e)). This application requires fair performances of the haptic display in producing both varying and constant force output. The proposed SmartSpring is capable of handling these requirements. We immersed a virtual ball into water using SmartSpring in this application, and reported the varying force with respect to time, as shown in Figure 13(b). We also plotted the displacement s measured by the sensor. It showed that SmartSpring well provided varying or constant forces under the jittery hand motion. Note that the force feedback in this application is commonly supported by active haptic devices. However, most passive devices are not able to provide the necessary rich force variation in this scenario.

Virtual Musical Instrument. Each configuration x of the control sliders in SmartSpring corresponds to a force-displacement characteristic, which can be seen as a native stiffness feature of SmartSpring. If we treat SmartSpring as a fully passive proxy, it has the properties similar to encountered-type haptics [52]. In this case, if we do not fix the end-effector of SmartSpring to user's hands, the user can place the hand on the pad with a proper timing during the interaction to perceive encountered-type haptics. By combining the configurable stiffness and encountered-type interaction, we can apply SmartSpring to operate as the musical instruments with multiple configurations. Users are

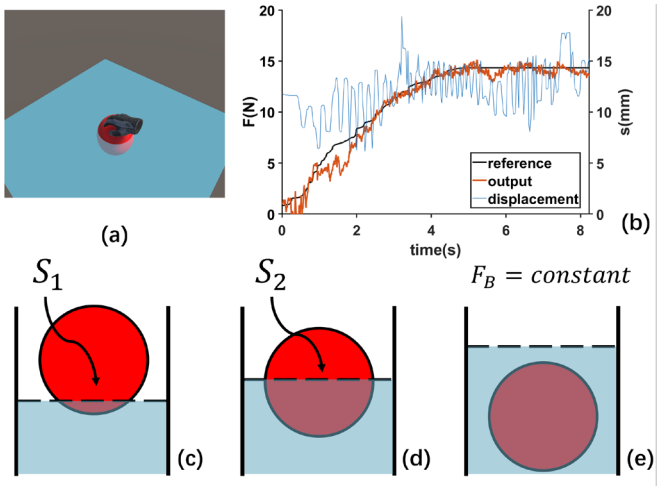

Fig. 13: (a) The virtual environment to render a buoyant force. (b) The collected desired force (black), feedback force (red) and the hand displacement signals (blue). (c,d) When the ball is immersed into the water, the cross-section area is varying with the depth of the ball increases, producing varying force signals. (e) When the ball is fully immersed, the system asks for rendering constant force feedback.

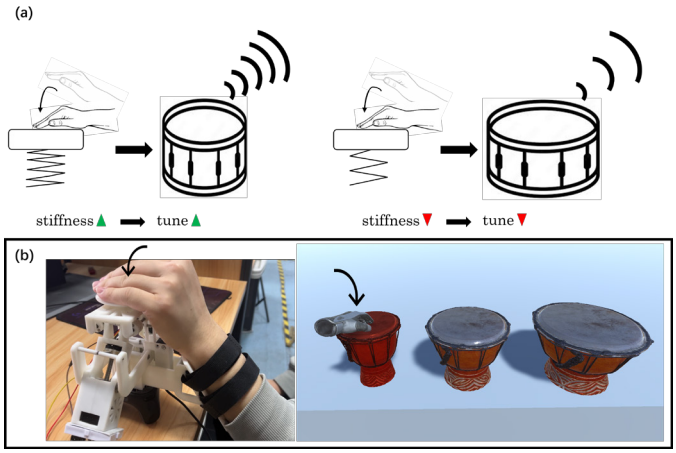

Fig. 14: (a) The SmartSpring operates as the drums with different levels of stiffness. (b) SmartSpring stably provides the haptic feedback corresponding to the VR scene.

allowed to pat it like playing hand drums. As shown in Figure 14, by enlarging the native stiffness through an increase in the length of x, the user can pat the high-stiffness display, similar to patting a "hard" drum that produces a high-pitched sound. Similarly, the low stiffness device acts like a "soft" drum that produces a low-pitched sound. As for the interaction in VR, the virtual environment detects whether the hand pats the drums and feeds the corresponding visual and audio cues to the user, along with the haptic feedback from SmartSpring.

7 Discussion, Limitation and Future Works

In this work, we developed a prototype with the design parameters listed in Table 5. The design parameters of our device were carefully chosen to meet various considerations, such as the desired force range, displacement capabilities, motor selection, standard part dimensions, and manufacturing feasibility. In the development of our current prototype, we manually determined these design parameters to ensure that all components are readily available for purchase or can be easily 3D printed. To aid in the design process, we employed the theoretical model that allowed us to simulate and evaluate the performance metrics of our design efficiently. This model also served for fine-tuning the design parameters and optimizing the overall performance of the device. Furthermore, the flexibility of our design allows for adjustments to the relevant parameters to accommodate different haptic display requirements. For example, if we employ stiffer springs and more powerful motors, the working range of SmartSpring will increase. It is also worthwhile to explore the development of computational design tools [53] for intelligent selection of design parameters. Additionally, while the workspace of SmartSpring is competitive, as presented in Table 1, the current output range of the device tends to display mild haptic feedback, such as elastic forces. We acknowledge that this limitation restricts the device's applications in VR environments. In future, we plan to address this limitation by incorporating a locking mechanism, which can fix the pad at desired poses to render rigid bodies and objects with mixed materials.

We exploited SmartSpring to provide force, stiffness, or torque feedback. The reported working range listed in Table 2 was tested for each interaction mode individually. When testing the torque display mode, we also did not quantitatively report the influence of the rotation angle θ. In our experience, a large rotation angle θ may decrease the accuracy of the feedback torque. However, in our user experiments, users did not need to actively rotate the pad to perceive the torque, and we did not observe large rotational angle during VR interactions. Note that if the force and torque feedback are simultaneously provided, the working range will depend on different configurations due to the coupling effects. We will study the coupled feedback of force and torque signals in the future. At present, SmartSpring can provide one-DOF force and one-DOF torque feedback. However, we will further explore methods for optimizing the kinematic structure to generating force/torque feedback with more DOFs.

The dynamic performance of SmartSpring is heavily dependent on the capacity of the motors. While high-end servomotor featuring closed-loop control could increase the dynamic performance, we have opted not to utilize them in this work. Instead, we prefer lightweight and cost-effective stepper motors, as they are more suitable for wearable haptic applications. Although the control sliders take approximately 0.67 seconds to complete the full stroke. The using experience demonstrates a reasonable dynamic performance for VR applications, where force signals are generally continuous. During our testing, we found a sense of hysteresis when rapidly pressing the touching pad. However, this behavior represents an extreme case unlikely to occur during typical VR interaction sessions. In our experiments from previous sections, we did not observe any significantly delayed experience in force feedback, which was also supported by the results of Q4 in section 5. Additionally, although the proposed hybrid spring-linkage provides fair stability in the open-loop control, we should note that there are still high frequency artifacts present. These unnatural jitters are reflected in the haptic distributions of Figure 6 (b)(d) and the fluctuation of Figure 13 (b). It is worth mentioning that the impact of these jitters is deemed insignificant, as reflected by the results of Q2 in section 5. Furthermore, the range of stiffness provided by our system is also dependent on its dynamic performance. Because stiffness is essentially the varied force output with respect to the motion, a higher dynamic performance corresponds to a larger range of the provided stiffness feedback. We will also improve the dynamic performance and analyze the range of stiffness feedback in the future.

Regarding the dimension and weight of our SmartSpring prototype, it measures $23 \times 7 \times 15$cm and weighs approximately 710 g, which is relatively big and heavy and might impact the wearability partly. However, during our experiments, we found the weight to be manageable, and no participants in our user study complained about the weight. Nevertheless, we recognize that a more compact and more lightweight design would be desirable for long-term use of our device. It is worth noting that the current weight of the two stepper motors used in the prototype accounts for 42% of the total weight, which limits the possibility for further size reduction. One potential solution is replacing the stepper motors with lighter and smaller actuators. In the future, we plan to investigate the use of tendons or electromagnetics to control the slider. In the other hand, the proposed spring-linkage structures is assembled symmetrically, a more compact design may be obtained

by the staggered layout after overcoming the problems of structural interference. Additionally, due to the self-weight of SmartSpring, force feedback may vary depending on the device's pose. In this study, we calibrated the system when it was up-oriented. To more effectively account for its self-weight, we plan to explore learning-based methods for calibrating the device under various poses.

Regarding the experiments, we presented the performance of SmartSpring and its potential in VR. While the results were fair, there are several points that are worth discussing and improving upon in future. In the variable-output experiments, SmartSpring performed with high generality in producing non-linear outputs. We should still note that all the presented curves in Figure 9 fall within the workspace shown in Figure 6 (a). This explains why all the variable-output curves show an increasing trend from small to large output. In the user study, we utilized confusion matrices to illustrate the performance of SmartSpring in terms of perception. The results were consistent with the practical experience of using the device. However, these matrices data obtained from the procedure of ranking order might be disturbed by various factors, such as the spacing and number of haptic stimuli. To address, the JND analysis further provides more information about the perceived haptic stimuli. In the future, a more comprehensive experiment will be established to validate the capabilities of SmartSpring. As for participants, SmartSpring has only been used by healthy right-handed youth in user study in this work. It is also necessary to have a large population with higher diversity to test our device before promoting the design to more users.

8 Conclusion and Future Work

In this paper, we propose the SmartSpring, a wearable low-cost haptic VR display capable of generating passive force, stiffness and torque feedback. By manipulating a spring-linkage structure, SmartSpring facilitates the rendering of continuous force and torque signals for VR scenes. Leveraging the passive structure, the proposed device works stably under involuntary hand movements. We validate the capability of SmartSpring in producing constant and variable outputs through quantitative experiments and conduct user studys to verify the perceptual experience of the proposed device.

In this work, we show the potential of adapting springs in dynamic passive structures to provide controllable haptic feedback. This is our first step to play with springs in the design of haptic displays for VR interactions. We will continue studying how to equip passive devices with springs to improve the force feedback across more DOFs. It is also interesting to explore methods of customizing SmartSpring for applications with distinct requirements regarding the force range and dynamic performance. Moreover, developing a miniaturized version of SmartSpring is a worthwhile endeavor to bring our design closer to affordable products for a broader range of applications in VR, AR, and MR in the future.

Acknowledgments

The authors would like to thank anonymous reviewers for their valuable comments. This work has been supported by the NSFC under Grants No.92148205, 62133009, 62132017 and 62141217, the Natural Science Foundation of Jiangsu Province under Grants No. BK20211159, the Shandong Provincial Natural Science Foundation under Grants No. ZQ2022JQ32, the CIE-Tencent Robotics X Rhino-Bird Focused Research Program and the Fundamental Research Funds for the Central Universities.

References

[1] Emanuel Sousa, Nuno Sousa, Rosane Sampaio, Joana Vieira, Marcelo Pires, Diogo Aguiam, Alar Ainla, João Gaspar, Gabriel Ribeiro, and Edoardo Sotgiu. Enhanced virtual reality application with tactile feedback for prototyping in-car dashboard surfaces. In *2021 IEEE World Haptics Conference (WHC)*, pages 335–335. IEEE, 2021. 1

[2] Claudio Pacchierotti, Stephen Sinclair, Massimiliano Solazzi, Antonio Frisoli, Vincent Hayward, and Domenico Prattichizzo. Wearable haptic systems for the fingertip and the hand: Taxonomy, review, and perspectives. *IEEE Transactions on Haptics*, 10(4):580–600, 2017. 1

[3] Osama R Bilal, Vincenzo Costanza, Ali Israr, Antonio Palermo, Paolo Celli, Frances Lau, and Chiara Daraio. A flexible spiraling-metasurface as a versatile haptic interface. *Advanced Materials Technologies*, 5(8):2000181, 2020. 1

[4] Arianna Mazzotta, Marco Carlotti, and Virgilio Mattoli. Conformable on-skin devices for thermo-electro-tactile stimulation: Materials, design, and fabrication. *Materials Advances*, 2(6):1787–1820, 2021. 1

[5] Mengjia Zhu, Shantonu Biswas, Stejara Iulia Dinulescu, Nikolas Kastor, Elliot Wright Hawkes, and Yon Visell. Soft, wearable robotics and haptics: Technologies, trends, and emerging applications. *Proceedings of the IEEE*, 110(2):246–272, 2022. 1

[6] Alex Mazursky, Shan-Yuan Teng, Romain Nith, and Pedro Lopes. Magnetio: Passive yet interactive soft haptic patches anywhere. In *Proceedings of the 2021 CHI Conference on Human Factors in Computing Systems*, pages 1–15, 2021. 1

[7] Inrak Choi, Eyal Ofek, Hrvoje Benko, Mike Sinclair, and Christian Holz. Claw: A multifunctional handheld haptic controller for grasping, touching, and triggering in virtual reality. In *Proceedings of the 2018 CHI conference on human factors in computing systems*, pages 1–13, 2018. 1

[8] Anatole Lécuyer. Simulating Haptic Feedback Using Vision: A Survey of Research and Applications of Pseudo-Haptic Feedback. *Presence: Teleoperators and Virtual Environments*, 18(1):39–53, February 2009. 1

[9] Huichan Zhao, Aftab M Hussain, Ali Israr, Daniel M Vogt, Mihai Duduta, David R Clarke, and Robert J Wood. A wearable soft haptic communicator based on dielectric elastomer actuators. *Soft robotics*, 7(4):451–461, 2020. 1

[10] Gabriele Frediani and Federico Carpi. Tactile display of softness on fingertip. *Scientific reports*, 10(1):20491, 2020. 1, 2

[11] Kahye Song, Sung Hee Kim, Sungho Jin, Sohyun Kim, Sunho Lee, Jun-Sik Kim, Jung-Min Park, and Youngsu Cha. Pneumatic actuator and flexible piezoelectric sensor for soft virtual reality glove system. *Scientific reports*, 9(1):8988, 2019. 1, 2

[12] Inrak Choi, Elliot W Hawkes, David L Christensen, Christopher J Ploch, and Sean Follmer. Wolverine: A wearable haptic interface for grasping in virtual reality. In *2016 IEEE/RSJ International Conference on Intelligent Robots and Systems (IROS)*, pages 986–993. IEEE, 2016. 1, 2

[13] Hugh Boys, Gabriele Frediani, Michele Ghilardi, Stefan Poslad, James C Busfield, and Federico Carpi. Soft wearable non-vibratory tactile displays. In *2018 IEEE International Conference on Soft Robotics (RoboSoft)*, pages 270–275. IEEE, 2018. 1, 2

[14] Gabriele Frediani, Hugh Boys, Michele Ghilardi, Stefan Poslad, James JC Busfield, and Federico Carpi. A soft touch: wearable tactile display of softness made of electroactive elastomers. *Advanced Materials Technologies*, 6(6):2100016, 2021. 1, 2, 4

[15] Takehito Kikuchi, Junichi Noma, Syuichi Akaiwa, and Yuya Ueshima. Response time of magnetorheological fluid–based haptic device. *Journal of Intelligent Material Systems and Structures*, 27(7):859–865, 2016. 1

[16] Yong Hae Heo, Dong-Soo Choi, In-Ho Yun, and Sang-Youn Kim. A tiny haptic knob based on magnetorheological fluids. *Applied Sciences*, 10(15):5118, 2020. 1

[17] Ronan Hinchet, Velko Vechev, Herbert Shea, and Otmar Hilliges. Dextres: Wearable haptic feedback for grasping in vr via a thin form-factor electrostatic brake. In *Proceedings of the 31st Annual ACM Symposium on User Interface Software and Technology*, pages 901–912, 2018. 1, 8

[18] Robert Kovacs, Eyal Ofek, Mar Gonzalez Franco, Alexa Fay Siu, Sebastian Marwecki, Christian Holz, and Mike Sinclair. Haptic pivot: On-demand handhelds in vr. In *Proceedings of the 33rd Annual ACM Symposium on User Interface Software and Technology*, pages 1046–1059, 2020. 2, 4

[19] Jinung An and Dong-Soo Kwon. Stability and performance of haptic interfaces with active/passive actuators—theory and experiments. *The International Journal of Robotics Research*, 25(11):1121–1136, 2006. 2

[20] Andre Zenner and Antonio Krüger. Shifty: A weight-shifting dynamic passive haptic proxy to enhance object perception in virtual reality. *IEEE transactions on visualization and computer graphics*, 23(4):1285–1294, 2017. 2

[21] André Zenner, Kristin Ullmann, and Antonio Krüger. Combining dynamic passive haptics and haptic retargeting for enhanced haptic feedback in virtual reality. *IEEE Transactions on Visualization and Computer Graphics*, 27(5):2627–2637, 2021. 2

[22] André Zenner and Antonio Krüger. Drag: on: A virtual reality controller providing haptic feedback based on drag and weight shift. In *Proceedings of the 2019 CHI Conference on Human Factors in Computing Systems*, pages 1–12, 2019. 2

[23] Daniel Martin, Sandra Malpica, Diego Gutierrez, Belen Masia, and Ana Serrano. Multimodality in vr: A survey. *ACM Computing Surveys (CSUR)*, 54(10s):1–36, 2022. 2

[24] Dangxiao WANG, Yuan GUO, Shiyi LIU, Yuru ZHANG, Weiliang XU, and Jing XIAO. Haptic display for virtual reality: progress and challenges. *Virtual Reality & Intelligent Hardware*, 1(2):136–162, 2019. 2

[25] Vincent Hayward and Karon E. Maclean. Do it yourself haptics: part i. *IEEE Robotics & Automation Magazine*, 14(4):88–104, 2007. 2

[26] Arata Horie, MHD Yamen Saraiji, Zendai Kashino, and Masahiko Inami. Encounteredlimbs: A room-scale encountered-type haptic presentation using wearable robotic arms. In *2021 IEEE Virtual Reality and 3D User Interfaces (VR)*, pages 260–269, 2021. 2

[27] Muhammad Abdullah, Minji Kim, Waseem Hassan, Yoshihiro Kuroda, and Seokhee Jeon. Hapticdrone: An encountered-type kinesthetic haptic interface with controllable force feedback: Example of stiffness and weight rendering. In *2018 IEEE Haptics Symposium (HAPTICS)*, pages 334–339, 2018. 2

[28] Shigeo Yoshida, Yuqian Sun, and Hideaki Kuzuoka. Pocopo: Handheld pin-based shape display for haptic rendering in virtual reality. In *Proceedings of the 2020 CHI Conference on Human Factors in Computing Systems*, pages 1–13, 2020. 2

[29] Hrvoje Benko, Christian Holz, Mike Sinclair, and Eyal Ofek. Normaltouch and texturetouch: High-fidelity 3d haptic shape rendering on handheld virtual reality controllers. In *Proceedings of the 29th annual symposium on user interface software and technology*, pages 717–728, 2016. 2

[30] Cathy Fang, Yang Zhang, Matthew Dworman, and Chris Harrison. Wireality: Enabling complex tangible geometries in virtual reality with worn multi-string haptics. In *Proceedings of the 2020 CHI Conference on Human Factors in Computing Systems*, pages 1–10, 2020. 2

[31] Steeven Villa Salazar, Claudio Pacchierotti, Xavier de Tinguy, Anderson Maciel, and Maud Marchal. Altering the stiffness, friction, and shape perception of tangible objects in virtual reality using wearable haptics. *IEEE Transactions on Haptics*, 13(1):167–174, 2020. 2, 4

[32] Shan-Yuan Teng, Tzu-Sheng Kuo, Chi Wang, Chi-huan Chiang, Da-Yuan Huang, Liwei Chan, and Bing-Yu Chen. Pupop: Pop-up prop on palm for virtual reality. In *Proceedings of the 31st Annual ACM Symposium on User Interface Software and Technology*, pages 5–17, 2018. 2

[33] Eric Whitmire, Hrvoje Benko, Christian Holz, Eyal Ofek, and Mike Sinclair. Haptic revolver: Touch, shear, texture, and shape rendering on a reconfigurable virtual reality controller. In *Proceedings of the 2018 CHI conference on human factors in computing systems*, pages 1–12, 2018. 2

[34] Humphrey Yang, Tate Johnson, Ke Zhong, Dinesh Patel, Gina Olson, Carmel Majidi, Mohammad Islam, and Lining Yao. ReCompFig: Designing Dynamically Reconfigurable Kinematic Devices Using Compliant Mechanisms and Tensioning Cables. In *CHI Conference on Human Factors in Computing Systems*, pages 1–14, New Orleans LA USA, April 2022. ACM. 2

[35] Lifeng Zhu, Xudong Jiang, Jiangwei Shen, Heng Zhang, Yiting Mo, and Aiguo Song. TapeTouch: A Handheld Shape-changing Device for Haptic Display of Soft Objects. *IEEE Transactions on Visualization and Computer Graphics*, 28(11):3928–3938, November 2022. 2

[36] Neung Ryu, Woojin Lee, Myung Jin Kim, and Andrea Bianchi. Elastick: A handheld variable stiffness display for rendering dynamic haptic response of flexible object. In *Proceedings of the 33rd Annual ACM Symposium on User Interface Software and Technology*, pages 1035–1045, 2020. 2, 8

[37] Jotaro Shigeyama, Takeru Hashimoto, Shigeo Yoshida, Takuji Narumi, Tomohiro Tanikawa, and Michitaka Hirose. Transcalibur: A weight shifting virtual reality controller for 2d shape rendering based on computational perception model. In *Proceedings of the 2019 CHI Conference on Human Factors in Computing Systems*, pages 1–11, 2019. 2

[38] Yongseok Lee, Somang Lee, and Dongjun Lee. Wearable haptic device for stiffness rendering of virtual objects in augmented reality. *Applied Sciences*, 11(15), 2021. 2

[39] Saurabh Jadhav, Mohamad Ramzi Abdul Majit, Benjamin Shih, Jürgen P Schulze, and Michael T Tolley. Variable stiffness devices using fiber jamming for application in soft robotics and wearable haptics. *Soft Robotics*, 9(1):173–186, 2022. 2

[40] Inrak Choi, Heather Culbertson, Mark R. Miller, Alex Olwal, and Sean Follmer. Grabity: A wearable haptic interface for simulating weight and grasping in virtual reality. In *Proceedings of the 30th Annual ACM Symposium on User Interface Software and Technology*, UIST '17, page 119–130, New York, NY, USA, 2017. Association for Computing Machinery. 2

[41] Evan Strasnick, Christian Holz, Eyal Ofek, Mike Sinclair, and Hrvoje Benko. Haptic links: Bimanual haptics for virtual reality using variable stiffness actuation. In *Proceedings of the 2018 CHI Conference on Human Factors in Computing Systems*, pages 1–12, 2018. 2

[42] Shuangyi Wang, Richard James Housden, Yohan Noh, Anisha Singh, Lukas Lindenroth, Hongbin Liu, Kaspar Althoefer, Joseph Hajnal, Davinder Singh, and Kawal Rhode. Analysis of a customized clutch joint designed for the safety management of an ultrasound robot. *Applied Sciences*, 9(9):1900, 2019. 2

[43] Ryosuke Tsumura and Hiroyasu Iwata. Robotic fetal ultrasonography platform with a passive scan mechanism. *International Journal of Computer Assisted Radiology and Surgery*, 15:1323–1333, 2020. 2

[44] Chan Lee, Suhui Kwak, Jihoo Kwak, and Sehoon Oh. Generalization of series elastic actuator configurations and dynamic behavior comparison. *Actuators*, 6(3):26, 2017. 2

[45] Mike Sinclair, Eyal Ofek, Mar Gonzalez-Franco, and Christian Holz. Capstancrunch: A haptic vr controller with user-supplied force feedback. In *Proceedings of the 32nd annual ACM symposium on user interface software and technology*, pages 815–829, 2019. 2, 3, 4

[46] Mohammad I. Awad, Dongming Gan, Irfan Hussain, Ali Az-Zu'bi, Cesare Stefanini, Kinda Khalaf, Yahya Zweiri, Jorge Dias, and Lakmal D. Seneviratne. Design of a novel passive binary-controlled variable stiffness joint (bpvsj) towards passive haptic interface application. *IEEE Access*, 6:63045–63057, 2018. 2, 8

[47] Ehsan Basafa, M Sheikholeslami, A Mirbagheri, F Farahmand, and GR Vossoughi. Design and implementation of series elastic actuators for a haptic laparoscopic device. In *2009 Annual International Conference of the IEEE Engineering in Medicine and Biology Society*, pages 6054–6057. IEEE, 2009. 3

[48] Ronald Van Ham, Thomas G Sugar, Bram Vanderborght, Kevin W Hollander, and Dirk Lefeber. Compliant actuator designs. *IEEE Robotics & Automation Magazine*, 16(3):81–94, 2009.

[49] X. Bao, S. Wang, R. Housden, J. Hajnal, and K. Rhode. A constant-force end-effector with online force adjustment for robotic ultrasonography. *IEEE Robotics and Automation Letters*, 6(2):2547–2554, 2021. 3

[50] Colin Swindells, Alex Unden, and Tao Sang. Torquebar: An ungrounded haptic feedback device. In *Proceedings of the 5th International Conference on Multimodal Interfaces*, ICMI '03, page 52–59, New York, NY, USA, 2003. Association for Computing Machinery. 7

[51] Pavel Senin. Dynamic time warping algorithm review. *Information and Computer Science Department University of Hawaii at Manoa Honolulu, USA*, 855(1-23):40, 2008. 8

[52] Víctor Rodrigo Mercado, Maud Marchal, and Anatole Lécuyer. "haptics on-demand": A survey on encountered-type haptic displays. *IEEE Transactions on Haptics*, 14(3):449–464, 2021. 8

[53] Adriana Schulz, Harrison Wang, Eitan Grinspun, Justin Solomon, and Wojciech Matusik. Interactive exploration of design trade-offs. *ACM Transactions on Graphics (TOG)*, 37(4):1–14, 2018. 9

A Appendix

We illustrate the kinematic model design of the SmartSpring here in detail. In our derivation, we will reuse the symbols in Figure 2. In the initial state, the end-effector is in the fixed initial position whose displacement s is set to 0. When the end-effector is pressed down and the displacement increases, two spring structures are extended to output elastic forces. Firstly, assuming the output force from one spring structure directs vertically up, as shown in Figure 2(a), the torque balance equation on the line AD' is written as

$$F_p L_b \sin(\alpha+\beta) - x F_s \sin\varphi = 0 \tag{5}$$

where F_p is the output force of the spring structure, L_b represents the length of rod AD', the $\alpha+\beta$ is the angle between AB and AD', in which α is the angle in the initial state, and β varies with respect to the displacement of the end-effector. x is the length of AC' which is controlled by the position of the slider and φ is the angle between BC' and AC'. According to the law of sines in the triangle ABC' and the Hooke's law in springs, we have

$$\frac{L_f}{\sin\varphi} = \frac{L_{sc}}{\sin(\alpha+\beta)} \tag{6}$$

$$F_s = F_0 + k(L_{sc} - L_{so}) \tag{7}$$

Table 5: Design parameters used in our prototype

Parameters	Value
The length of the rod AC x	9 mm - 30 mm
The length of the link AD L_b	60 mm
The length of the frame AB L_f	35 mm
The length of the AF L_h	73.5 mm
The length of the EF L_v	50.5 mm
The vertical displacement of the pad s	0 mm - 25 mm
The initial angle between AB and AC' α	34°
The rotation angle of the pad θ	-27.5°- 27.5°
The force arm l	18 - 42 mm
The rest length of the spring	20 mm
The stiffness of the spring k	1.3 N/mm

where L_f is the constant length of frame AB, L_{sc} is the length of the spring after the end-effector is pressed, L_{so} is the spring length in the initial state. The L_{so} is longer than the native length of the spring so that it provides an initial force F_0. k is the constant stiffness of the spring. According to Equation 6 and Equation 7, the relation between output force and the extension of spring is

$$F_p = \frac{xL_f}{L_b L_{sc}}(F_0 + k(L_{sc} - L_{so})). \tag{8}$$

According to the geometric constraints, L_{sc} and the displacement of end-effector s are respectively represented as

$$L_{sc} = \sqrt{x^2 + L_f^2 - 2xL_f\cos(\alpha+\beta)} \tag{9}$$

$$s = L_b(\cos\alpha - \cos(\alpha+\beta)) \tag{10}$$

Substituting Equation 9 and Equation 10 into Equation 8, the output force is

$$F_p = k\frac{xL_f}{L_b} + \frac{xL_f}{L_b}\cdot\frac{F_0 - kL_{so}}{T}, \tag{11}$$

$$T = \sqrt{x^2 + L_f^2 - 2dL_f(\cos\alpha - s/L_b)} \tag{12}$$

In these parameters from Equation 11 and Equation 12, $\{L_b, L_f, \alpha, k, F_0\}$ is the set of design parameters which are determined in the design process. s is measured by the displacement sensor in real-time. According to the variable s, the motor controls x to output the desired force F_p.

When the two sliders are constrained to work symmetrically, the output forces from the two springs are balanced along the horizontal direction. Therefore, the output force on the pad P is computed as

$$F = 2F_p. \tag{13}$$

When the two sliders are allowed to move asymmetrically, the output forces from the two springs are different. They will provide a torque on the pad P. In this mode without constraining the rotation motion of the pad P, it will generally have an angle θ deviated from the horizontal direction when the hand casually hold the pad, as illustrated in Figure 2(d). In this case, the output forces of two springs and the rotation angles of two rods are different. Here we use subscripts i = 1 and 2 to represent components at the left and right sides respectively. Because the force-generating units are mirror-symmetric, if the rotation of the pad to the left unit θ_1 is θ, we have the pad rotation to the right unit $\theta_2 = -\theta$. The rotation angles of the two rods $\alpha+\beta_1$ and $\alpha+\beta_2$ are then computed by

$$\frac{L_v - s - L_b\cos(\alpha+\beta_i)}{L_h - L_b\sin(\alpha+\beta_i)} = \tan\theta_i \tag{14}$$

Due to the rotation angle θ of the pad, the output force from one spring F_p' after rotation is

$$F_{p_i}' = F_{p_i}\frac{\sin(\alpha+\beta_i)}{\sin(\alpha+\beta_i+\theta_i)} \tag{15}$$

Substituting Equation 11 to Equation 15, we will obtain the output force F_{p_i}' for cases when the pad is rotated. From the geometry of the diagram, the force arms l_i of the pair of force F_{p_i}' are represented as:

$$l_i = \frac{L_h - L_b\sin(\alpha+\beta_i)}{\cos\theta} \tag{16}$$

and the output torque M is finally obtained as:

$$M = F_{p_2}' l_2 - F_{p_1}' l_1 \tag{17}$$

The detailed design parameters of our SmartSpring prototype used in experiments are listed in Table 5.